

Dynamic symmetrical pattern projection based laser triangulation sensor for precise surface position measurement of various material types

Klemen Žbontar,^{1,*} Matjaž Mihelj,² Boštjan Podobnik,¹ Franc Povše,¹ and Marko Munih²

¹LPKF Laser & Elektronika, D. O. O., Polica 33, 4202, Naklo, Slovenia

²Faculty of Electrical Engineering, University of Ljubljana, Tržaška 25, 1000, Ljubljana, Slovenia

*Corresponding author: klemen.zbontar@lpkf.si

Received 1 November 2012; revised 27 February 2013; accepted 8 March 2013;
posted 12 March 2013 (Doc. ID 179086); published 17 April 2013

This paper describes a custom, material-type-independent laser-triangulation-based measurement system that utilizes a high-quality ultraviolet laser beam. Laser structuring applications demand material surface alignment regarding the laser focus position, where fabrication conditions are optimal. Robust alignment of various material types was solved by introducing dynamic symmetrical pattern projection, and a “double curve fitting” centroid detection algorithm with subsurface scattering compensation. Experimental results have shown that the measurement system proves robust to laser intensity variation, with measurement bias lower than 50 μm and standard deviation lower than $\pm 6.3 \mu\text{m}$ for all materials. The developed probe has been integrated into a PCB prototyping system for material referencing purposes. © 2013 Optical Society of America

OCIS codes: (120.0120) Instrumentation, measurement, and metrology; (140.3610) Lasers, ultraviolet; (150.1135) Algorithms; (150.3045) Industrial optical metrology; (150.5670) Range finding; (280.3400) Laser range finder.

<http://dx.doi.org/10.1364/AO.52.002750>

1. Introduction

Prototyping is one of the most crucial steps in a product development process. It allows engineers to quickly test new ideas and easily incorporate changes. The printed circuit board (PCB) development process often makes use of this step as it validates simulation results, thus providing the best overview of product capabilities and its limitations. The trend of reducing board and structure dimensions requires an increase in prototype fabrication precision, which is achieved by a laser structuring process [1]. Structuring is carried out by means of a laser beam in focus, where the beam diameter is the smallest and its optical power is the greatest. Beam divergence, caused by the optical configuration, defines boundaries around the focus point, within which the laser structuring process is still carried out effectively.

Optimal material positioning relative to the laser focus point plays an important role in achieving the desired fabrication tolerances. Alignment could be incorporated with an online measuring system, which has to enable robust measurement of a variety of possible prototyping materials. The measurement accuracy should be lower than the beam's Rayleigh length. This problem could be solved by using commercially available contact or contactless displacement sensors. The former provide high accuracy and repeatability, and show robustness to material surface properties. On the other hand, they need to be mounted above the measurement point, which coincides with the laser beam. The latter can be mounted outside the laser's working area, but they lack robustness to material type. Transparent materials present the greatest drawback since only a small amount of incident light gets reflected from the surface while the rest penetrates through the material.

In order to satisfy the aforementioned requirements (robust measurement of different material types with high measurement precision under

1559-128X/13/122750-11\$15.00/0
© 2013 Optical Society of America

100 μm), a custom contactless displacement sensor based on a laser beam was developed. Development of a sensor with such strict requirements demands knowledge of possible operation principles and their limitations [2]. Laser triangulation provides a contactless measurement method that allows the sensor to be mounted outside the laser's working area. Understanding of different sources of measurement uncertainty is required [3]. Possible sources of uncertainty include sensor geometry [4], laser beam dimension [5], and beam scattering [6]. The fundamental source of measuring uncertainty is speckle noise which arises because of interference of scattered wave fronts from a microscopically rough surface [7]. This limitation was thoroughly studied and documented by Baribeau and Rioux [8,9] as well as Dorsch *et al.* [10]. They linked the uncertainty to multiple optical parameters and presented methods and design criteria for reducing its effect on the measurement result. The uncertainty is insensitive to linear filtering, but can be decreased using spatial integration of the detected signal. Sensitivity to surface properties could be reduced using beam dithering and static symmetrical pattern projection [3]. The latter approach reduces the effect of nonuniformly distributed light and surface damage, but does not affect speckle related uncertainty. Even simple linear dimensional measurement accuracy of well-defined objects is affected by a number of error sources [11,12]. Undesired secondary reflections from vertical surfaces are proven to present the dominant measurement error source.

The laser triangulation principle is used in a wide spectrum of applications. Zeng *et al.* [13] have developed a two-beam probe for tracking and measuring the position of a moving object. Curved, discontinuous surfaces with varying reflectance can be measured by analyzing the temporal signal of the reflected light [14]. The principle is also useful in medicine for measuring human vocal fold vibrations by analyzing the detected oval shape, which is caused by laser spot movement [15]. Additional optical elements could be used to project various patterns, such as a circle [16,17] or a line [18], thus solving diverse measurement problems. Combining a greater number of light detectors into a radially distributed array reduces errors due to material discontinuity and enables measurements of tilted surfaces [19,20]. Transparent materials present a limitation for classic laser triangulation probes due to the low absorption rate in the visible spectral range. Rantson *et al.* [21,22] have presented a method for acquiring the 3D shape of transparent objects using an ultraviolet (UV) laser source and a stereo vision scheme. The method is based on detecting fluorescent points generated by the absorption of the UV laser beam.

This paper presents a novel laser-triangulation-based measurement system that allows precise one-dimensional measurements of various material types [23]. It introduces dynamic symmetrical

pattern projection with the use of a scanning unit and an appropriate detection algorithm. This approach reduces the effect of errors related to the material surface, which affect the quality of the projected dot as seen in Fig. 1.

Furthermore, many authors have shown that spatial signal integration decreases measurement uncertainty related to speckle noise [3,9]. Measurement of transparent and translucent materials is enabled with the use of a high-quality UV laser beam, which is generally used for structuring purposes. In order to use it for measuring purposes, the laser source has to operate in continuous wave (CW) mode and its intensity has to be controlled accordingly.

The remainder of this paper is organized as follows: drawbacks of classic laser triangulation probes and the theoretical background of the developed detection method are presented in Section 2. Section 3 describes experiments conducted with varying laser intensities and different material types. The performance of the presented measurement system is discussed in Section 4, and the concluding remarks are presented in Section 5.

2. Methodology

The basic laser triangulation scheme consists of three main building blocks, all presented in Fig. 2. The developed measuring system utilizes a 2D CMOS light sensor with a resolution of 640×480 px and frame rate of 30 FPS. Reflected light is collected by a microscope objective whose specifications are presented in Table 1. The viewing axis of the detection system is aligned with the idle laser projecting axis. This step simplifies the processing algorithm because material movement is detected as signal movement in only one axis, as shown in Fig. 2. Thus, material position dZ with regard to a reference point can be expressed by

$$dZ = \frac{dz}{\sin \alpha} \frac{1}{\beta} = \frac{dz}{K} = \frac{dy}{K} = \frac{y_1 - y_0}{K} \quad (1)$$

where dz is the detected movement while α and β are the triangulation angle and the lens magnification, respectively. dZ is much smaller than the sensor standoff distance L ($dZ \ll L$). It should be carefully noticed in Eq. (1) that β does not denote a constant value as it is affected by radial lens distortion. Hence,

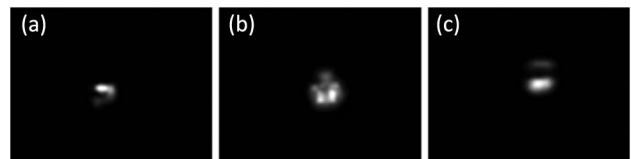


Fig. 1. Effects of material surface discontinuities and optical properties on the shape of the acquired signal. The acquired laser dot can have an irregular, discontinuous shape and uneven light intensity distribution, most often caused by surface scratches.

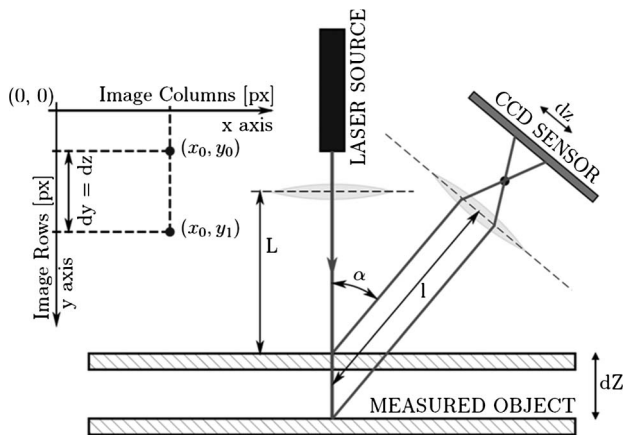


Fig. 2. Laser triangulation operating principle with the use of an aligned 2D light sensor. Optical alignment results in virtual laser dot movement in one axis, thus simplifying the detection algorithm.

the measurement system needs to be calibrated to compensate for this effect.

The laser projection system consists of a built-in high-quality UV laser source, a 2D scanning system used for laser beam deflection, and a telecentric scanning lens. The latter provides a flat working field at the image plane of the scanning system and defines the laser beam focus position.

Various properties of the material surface, such as reflection type, finishing, sharp edges, and texture discontinuities, govern the quality of the reflected spot. The incident laser beam is thus not reflected evenly from these areas, causing the acquired signal to have irregular, chunked shapes with an unevenly distributed intensity profile, Fig. 1. The problem can be solved by introducing dynamic symmetrical pattern projection, a circle with radius $r = 0.5$ mm in our case, using the 2D scanning system. In order to obtain a visually static pattern, the scanning speed has to be far greater than the camera acquisition speed (Fig. 3). As in projecting a dot, the processing algorithm has to robustly calculate the acquired pattern centroid, which serves as an intermediate result in material displacement calculation. This presented projection method has numerous advantages over simple dot projection. Even though material position is calculated from the illumination pattern displacement in the y axis, symmetric pattern projection could be described as a redundancy

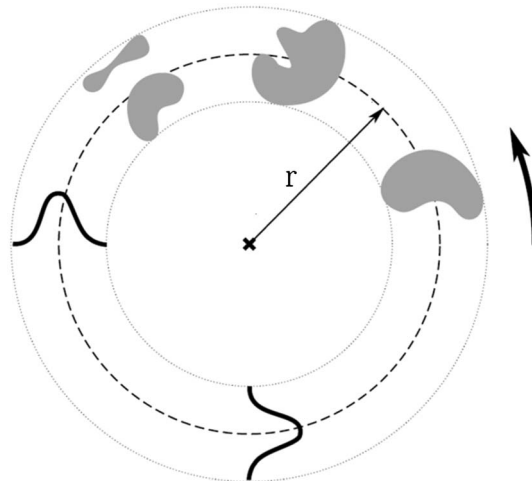


Fig. 3. Dynamic symmetrical pattern projection. High scanning speed enables spatial integration of the detected signal, thus resulting in Gaussian light intensity distribution when radial cross sections are examined.

that enables robust and precise centroid position detection [3]. Unlike projecting a line or even multiple lines, the circle shape results from continuous beam deflection. Thus, in an ideal case, the pattern has an evenly distributed light intensity profile. A larger active measurement area reduces the effect of local material surface irregularities.

Projected pattern symmetry enables a measurement result to be obtained even though some parts of the pattern have bad quality or are even not visible, as presented in Fig. 4. In combination with appropriate curve fitting, the presented approach results in a reduction of measurement errors related to the material surface. This is possible because the pattern geometry allows a precise centroid position to be obtained from corrupted or limited data. In addition, the simplicity of a circle pattern makes it robust to various errors. Nevertheless, other symmetrical patterns could also be used. Stripes, on the other hand, do not provide a sufficient level of robustness as their calculated position is dependent on a majority of aforementioned sources of error. Although the incident laser beam has low power, materials are subjected to UV irradiation, causing some of them to degenerate. The effect is clearly visible in the case of projecting a dot, where the shape and

Table 1. VC Technology Corporation Microscope Objective Specifications (SV-3518V)

Focal length	35 mm
Maximum aperture ratio	1:1.8
F -number	$F1.8 \sim$ Close
Max. sensor size (MSS)	16.96 mm
Radial distortion at MSS	-0.13%
Mount	C-mount
Iris & Focus	Manual

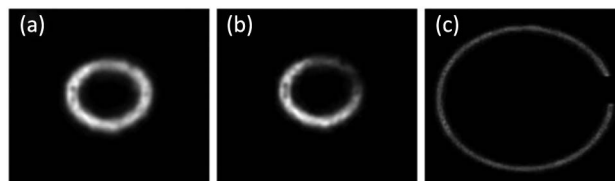


Fig. 4. Possible irregularities of dynamic circle projection. Detected signal with good quality (a), uneven distribution of light intensity caused by optical properties of the material (b), and unconnected pattern, resulting from insufficient scanning speed (c).

position of the detected signal vary randomly. This decreases the measurement precision and gradually changes the surface. Dynamic projection averages the incident optical power, thus reducing material degeneration and, in an ideal case, resulting in a Gaussian distribution of light intensity if radial cross sections of the acquired pattern are studied (Fig. 3). The mentioned method is known to reduce speckle noise and its effect on measurement uncertainty. Speckle noise is reduced by moving the measured material during acquisition time or, as in our case, by dynamically projecting a circle instead of a dot, which enables far greater movement speeds. In both cases, movement averages the interference of the scattered wave fronts.

Measurement precision is tightly dependent on the optimal laser beam intensity setting, because a thin circle adds less uncertainty to centroid calculation than a thick one. In an ideal case, the acquired pattern can be described as a connected curve with an evenly distributed light intensity. Any radial cross section of the acquired pattern shows a double Gaussian curve, which denotes opposite light intensity distributions. Because of a small circle radius, modifying the laser beam intensity changes the cross-section profiles accordingly, as shown in Fig. 5. The optimal laser beam intensity is achieved when two separate Gaussian curves are detected in the circle's cross-section profile. When we increase the laser beam intensity, an increase in curve widths is detected. On some surfaces, the two curves gradually merge into one, denoting a fully illuminated circle.

The triangulation angle transforms the projected circle into an ellipse which is detected by the camera. Robust centroid calculation is achieved using a "double curve fitting" (DCF) centroid detection method. It reduces the influence of aforementioned irregularities and improves measurement accuracy. The acquired image, which is obtained with a long

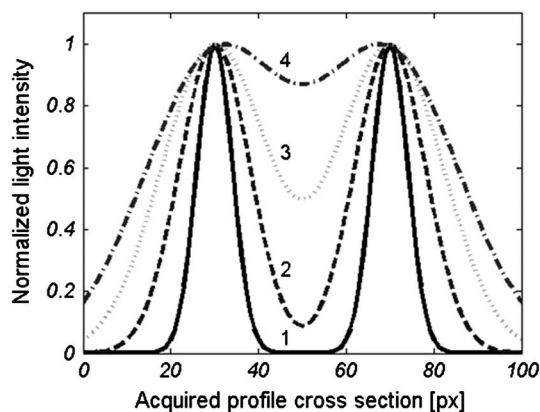


Fig. 5. Dependence of projected circle cross-section profiles on laser beam intensity. With optimal laser beam intensity, two separate Gaussian curves are visible (curve 1). Increasing the intensity value results in greater standard deviation of Gaussian curves (curves 2–4).

exposure time, is first processed by a 2D median filter with a 3×3 kernel. In the next step, we acquire an approximate ellipse centroid by calculating the average position of blobs which describe the pattern on a black-and-white image. The centroid position is highly dependent on the pattern illumination intensity distribution and may vary significantly from the "real" value but cannot be located outside the pattern. The approximate centroid is used as the rotation axis for calculating radial cross sections. These are obtained by calculating the rotation vector and interpolating the desired intensity values as presented in Fig. 6.

Cross-section points (x', y') can be expressed by

$$\begin{bmatrix} x' \\ y' \end{bmatrix} = \begin{bmatrix} \cos \theta & -\sin \theta \\ \sin \theta & \cos \theta \end{bmatrix} \begin{bmatrix} x \\ y \end{bmatrix} + \begin{bmatrix} x_0 \\ y_0 \end{bmatrix}, \quad (2)$$

where θ and (x_0, y_0) denote the rotation angle and the center of rotation respectively. The desired cross-section intensity values are obtained using bilinear interpolation

$$f(H_1) \approx \frac{x_2 - x_q}{x_2 - x_1} f(P_{11}) + \frac{x_q - x_1}{x_2 - x_1} f(P_{21}), \quad (3)$$

$$f(H_2) \approx \frac{x_2 - x_q}{x_2 - x_1} f(P_{12}) + \frac{x_q - x_1}{x_2 - x_1} f(P_{22}), \quad (4)$$

$$f(Q) \approx \frac{y_2 - y_q}{y_2 - y_1} f(H_1) + \frac{y_q - y_1}{y_2 - y_1} f(H_2), \quad (5)$$

where $f(Q)$ denotes the interpolated value at point $Q = (x_q, y_q)$.

The DCF method is based on analysis of the acquired pattern's radial cross sections, which are derived from the previously calculated approximate ellipse centroid. The cross sections are equally spaced and describe a whole circle as seen in Fig. 6(a). In the first fitting step, a Gaussian curve is fitted to each radial cross section, thus reducing measurement dependence on unevenly distributed

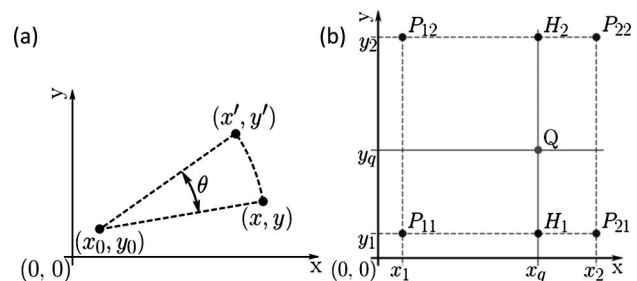


Fig. 6. Rotation of an arbitrary point around an arbitrary rotation axis (a) and bilinear interpolation (b).

ellipse illumination. The Gaussian distribution is defined by

$$I(r) = A \exp\left(-\frac{(r-b)^2}{2c^2}\right), \quad (6)$$

where A , b , and c denote the signal amplitude, mean, and standard deviation, respectively. This process results in an array of points, which depict the positions of fitted Gaussian curve peaks.

In the second fitting step, an ellipse is fitted to the calculated point set, thus eliminating separate point deviations. An ellipse with an arbitrary centroid is expressed by

$$0 = \frac{(x-x_0)^2}{a^2} + \frac{(y-y_0)^2}{b^2} - 1, \quad (7)$$

where a and b define the semi-major and semi-minor axes, respectively. The point (x_0, y_0) denotes the ellipse centroid, which represents the result of the DCF method.

Translucent materials, where the incident beam penetrates into the material surface, deserve special consideration. The theory of subsurface scattering from translucent materials is documented in [24–26]. Subsurface scattering in combination with the triangulation angle results in a drop-like shape of the acquired ellipse. When radial cross sections are studied, this irregularity is seen as a skewed Gaussian distribution of the light intensity (Fig. 7). Skewness is negligible in the x -axis direction and increases toward a maximum value in the y -axis direction. The skewed Gaussian distribution is expressed by

$$f(r, \sigma, \mu, \alpha) = \frac{1}{\sqrt{2\pi}\sigma} \exp\left(-\frac{(r-\mu)^2}{2\sigma^2}\right) \times \operatorname{erfc}\left(-\frac{\alpha(r-\mu)}{\sqrt{2\sigma}}\right), \quad (8)$$

$$\operatorname{erfc}(r) = 1 - \operatorname{erf}(r) = \frac{2}{\sqrt{\pi}} \int_r^\infty \exp(-t^2) dt, \quad (9)$$

where σ and μ denote the Gaussian distribution's standard deviation and mean, α depicts the skewness parameter and $\operatorname{erfc}(r)$ defines a complementary error function. The aforementioned DCF method results in false ellipse centroids since Gaussian curves do not accurately describe the radial intensity distribution, as seen in Figs. 7 and 8.

The effect of subsurface scattering can be reduced by using lower laser beam intensity, resulting in a smaller penetration depth. Additionally, we use the ellipse's symmetry to introduce subsurface scattering compensation. In an ideal case, any two opposite cross-section profiles relative to a symmetry line, which runs perpendicular to the viewing axis, are described with the same, but opposite skewness values. We first align these two profiles with regard to their peak positions and then perform a summation of the aligned profiles (Fig. 9). The result is thus described with a Gaussian-like curve, and its maximum value position coincides with the fitted Gaussian curve mean.

3. Results

Testing of the presented measurement system and the DCF processing algorithm was conducted on a prototyping series laser structuring machine, ProtoLaser U3, manufactured by LPKF Laser & Elektronika [1]. The measurement system was designed and developed with the aforementioned elements because all except the CMOS camera are already implemented on the prototyping system and used for the structuring process which significantly decreases production costs. The laser scribing process is carried out by a built-in high-quality diode UV laser source emitting a Gaussian beam with wavelength $\lambda = 355$ nm, beam waist radius $\omega_0 = 7.5$ μm and Rayleigh length $z_R = 498$ μm . During measurements, the laser system operates in CW mode, with low optical power, where the beam intensity is regulated by a built-in acousto-optic attenuator. The detection system is mounted at an angle

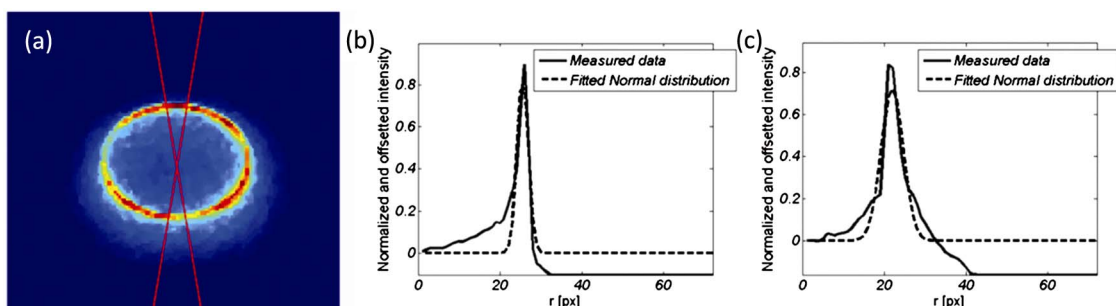


Fig. 7. Study of the subsurface scattering effect in translucent materials. Boundaries for averaging radial cross-section profiles around the vertical symmetry axis, where skewness is most visible (a). The resulting negative (b) and positive (c) skewness of light intensity distribution from the upper and lower half of the pattern, respectively. An offset between the measured curve and the fitted normal curve peak positions result in measurement errors.

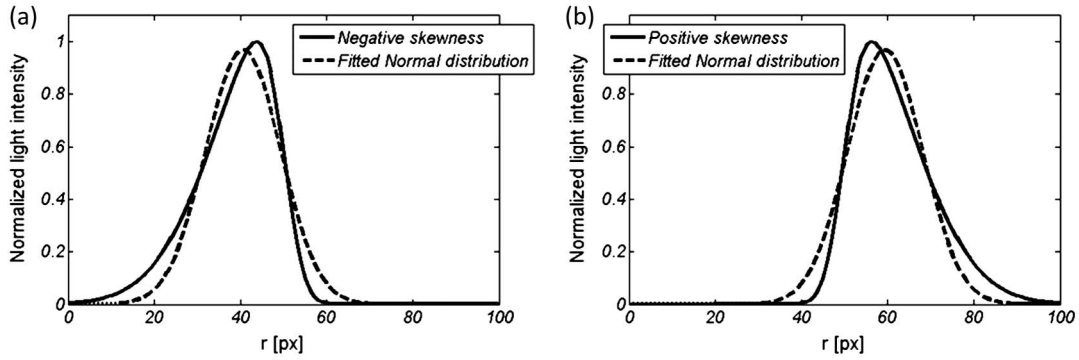


Fig. 8. Study of misalignment of peak positions between an ideal skewed normal curve and a fitted normal curve. Negative skewness results in an offset of the fitted normal curve peak toward the left (a) while positive skewness results in an offset of the fitted normal curve peak toward the right (b).

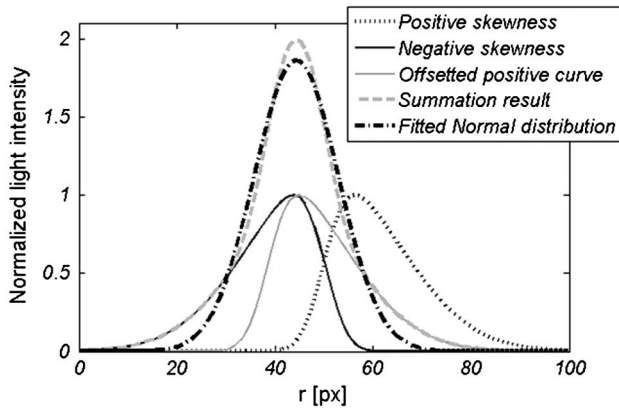


Fig. 9. Subsurface scattering compensation. In an ideal case, when studying opposite radial cross-section profiles, we obtain two equal but vertically mirrored skewed Gaussian light intensity distributions (solid curves). Summation of these profiles with regard to their peak value positions results in a Gaussian-like symmetrical curve (dash curve). The resulting curve peak and the fitted Gaussian curve (dash-dot curve) peak coincide.

$\alpha = 41^\circ$ and distance from measurement point $l = 167.5$ mm. The circle pattern is projected by a Newson active 2D scanner unit with projection resolution $res = 81.92$ step/mrad ($res = 1.147$ step/ μm) and projection speed $v_p = 1500$ mm/s. The

measured material is positioned on a moving orthogonal table with the z (vertical) axis resolution of ± 1 μm .

Throughout this paper, we evaluate and fit Gaussian curves to 90 radial cross-section profiles, equally spaced with an angle $\varphi = 4^\circ$. Prior to conducting other experiments, we verified the robustness of the DCF method to material type and surface irregularities. Different material types result in different reflection qualities, and surface damage such as scratches and wrinkles noticeably reduces the acquired pattern quality as seen in Fig. 10.

Figure 10 shows results of the DCF method with included subsurface scattering compensation for four representative material types: diffuse, translucent, transparent, and porous. One can notice that the aforementioned detection method is robust to material type and some surface damage, which is seen as unevenly distributed or discontinuous light intensity. Projection of a circle onto white paper results in a thin, evenly distributed pattern that is little-affected by surface irregularities. This material was thus chosen as a reference material. A reference point was set at the laser focus level, where optimum laser beam intensity (2.85 V) and the DCF method with subsurface scattering compensation were used.

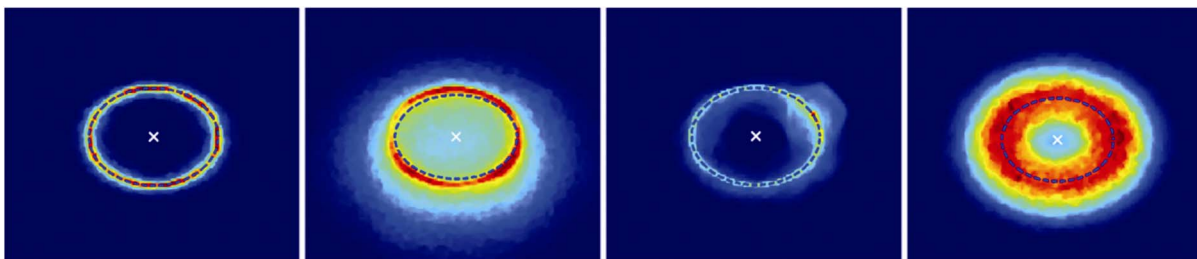


Fig. 10. Pattern symmetry property provides robustness to reflection type and material surface irregularities. Different material types: white paper, FR4, cover layer, and ceramics (left to right) result in different reflection types, which govern the acquired pattern quality. Red and blue color shades in the images represent high and low light intensities, respectively. The blue dashed curve represents the fitted ellipse and the white cross represents its centroid.

In the following experiments, we utilized a Keyence GT2-H12K contact sensor as a reference for positioning the measured materials. The sensor provides a 12 mm measuring range with 1 μm (peak–peak) accuracy and 0.1 μm measuring resolution. It was mounted parallel to the idle laser beam axis where an eccentric measurement tip allowed measurements to be conducted 3 mm from the projected circle pattern centroid. Prior to starting a measurement, we positioned each material surface relative to the previously defined reference point.

First, we evaluated the robustness of the DCF method to laser beam intensity variation and compared the performance of the method with and without subsurface scattering compensation. The measurements were conducted on a diffuse material (white paper) and on a translucent material (FR4) where an optimal intensity setting is crucial. For statistical reasons, each measurement result consists of the mean and standard deviation of 100 measurements. Measurement results for a diffuse material are presented in Fig. 11 and Table 2 (Appendix A).

The measurement method proves robust to laser intensity variations when measuring diffuse materials, as seen in Fig. 11 and Table 2. The two ellipse centroid detection methods (DCF with and without subsurface scattering compensation) provide comparable results. Careful consideration should be given to vertical axis boundaries when examining the results in Fig. 11. The method with compensation shows a small measurement bias and relatively high standard deviation, with a best result of $o_{b_{\text{comp}}} = 0.2 \pm 1.0 \mu\text{m}$ and a worst result of $o_{w_{\text{comp}}} = 1.8 \pm 5.3 \mu\text{m}$. Standard deviation values are found between $\pm 0.9 \mu\text{m}$ and $\pm 5.3 \mu\text{m}$. The method without compensation results in a greater measurement bias (which increases with increasing beam

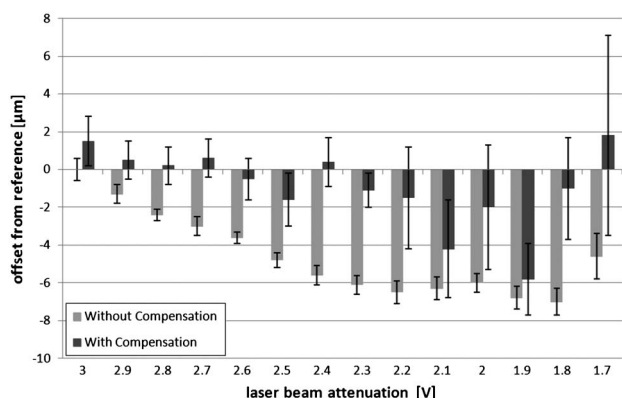


Fig. 11. Effect of laser beam intensity variation on diffuse (white paper) material measurement. The laser beam attenuation value governs the beam intensity. 3 V and 1 V depict the lowest and the highest allowed intensities, respectively. Both detection methods provide comparable results, though the DCF method without subsurface scattering compensation shows dependence on laser beam intensity.

intensity), and a lower, more constant standard deviation, with a best result of $o_b = -0.0 \pm 0.6 \mu\text{m}$ and a worst result of $o_w = -6.8 \pm 0.6 \mu\text{m}$. Standard deviation values are found between ± 0.6 and $\pm 2.4 \mu\text{m}$.

Translucent materials (in our case, FR4) present some problems due to partial laser beam penetration and consequential subsurface scattering. FR4 is a composite material consisting of woven fiberglass cloth and an epoxy resin binder. In the PCB manufacturing industry, it is used as a carrier layer for conductive copper coating. Measurement results for the translucent material are presented in Fig. 12 and Table 3 (Appendix A).

Figure 12 clearly shows the superior performance of the DCF method with subsurface scattering compensation. It shows robustness to laser intensity variation and the corresponding drop-like pattern shape, whereas the DCF method without subsurface scattering compensation results in strong dependence on laser intensity. The drop-like effect is clearly seen on the images presented in Table 3. Similarly to diffuse materials, the related measurement bias increases with increasing laser intensity and reaches a maximum at $o_w = -119.3 \pm 2.6 \mu\text{m}$. In comparison, the worst result with subsurface compensation method is $o_{w_{\text{comp}}} = -19.4 \pm 1.4 \mu\text{m}$. Furthermore, the standard deviation of the DCF method with subsurface scattering compensation is low and constant, with values reaching from ± 1.0 to $\pm 1.5 \mu\text{m}$. On the other hand, the other method results in higher standard deviation that is dependent on laser beam intensity, with values reaching from ± 1.7 to $\pm 7.3 \mu\text{m}$.

Furthermore, we conducted measurements on different prototyping materials to verify robustness to various surface properties. In order to obtain the values of fundamental measurement accuracy and repeatability, we set the optimum laser beam

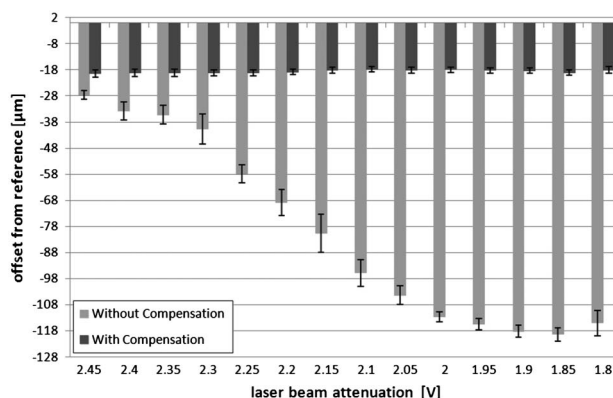


Fig. 12. Effect of laser beam intensity variation on translucent material (FR4) measurement. The laser beam attenuation value governs the beam intensity. 3 V and 1 V depict the lowest and the highest allowed intensities, respectively. The DCF method with subsurface scattering compensation provides superior measurement performance with constant measurement bias and high repeatability.

intensity for each material. For statistical reasons, each measurement result consists of the measurement bias and its standard deviation over 500 measurements. The results are presented in Fig. 13 and Table 4 (Appendix A). Figure 13 shows that the measurement accuracy and standard deviation are closely dependent on the measured material optical properties, which are denoted in Table 4. In most cases, the DCF method with subsurface scattering compensation provides better measurement accuracies, but results in higher standard deviation. We obtained the best measurement results when measuring materials that result in thin, evenly distributed circle patterns. These materials enable high measurement accuracy, with values located between -2.9 and -13.9 μm , and low standard deviation, ranging from ± 0.8 to ± 1.6 μm . Measurement of translucent materials results in a fundamental measurement bias caused by subsurface scattering. Thus, the detection method provides measurement accuracies between -20.9 and -28.9 μm and low standard deviation ranging from ± 1.6 to ± 1.7 μm . We obtained the worst results with materials that result in thick, unevenly distributed circle patterns. The measurement accuracy for such materials ranges from -30 to -43.5 μm , with high standard deviation from ± 5.5 to ± 6.3 μm . An exception is PTFE, which gives a high measurement bias of -29.6 μm and low standard deviation of ± 1.1 μm .

Finally, we conducted measurements of a statically positioned diffuse material (white paper) and a static laser dot which served as a comparison to the developed method's performance. The laser beam intensity was set to an optimal value (2.85 V) prior to starting the measurements. For statistical reasons, 100 measurement points were obtained and their standard deviation was calculated. The laser dot is subjected to all aforementioned irregularities, resulting in a standard deviation of ± 11.1 μm . The

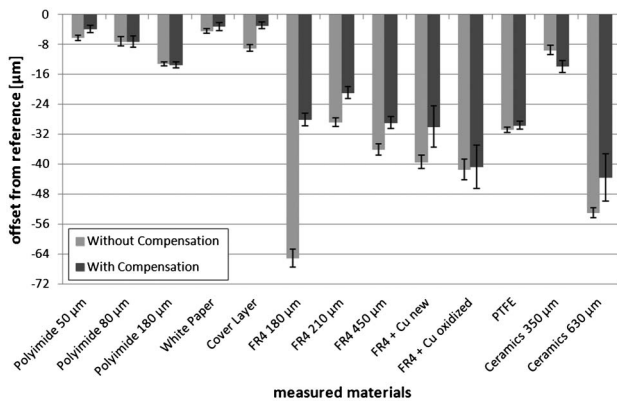


Fig. 13. Effect of different material types on measuring performance. The measurements were conducted under optimum laser beam intensity regarding each material. Measurement performance is dependent on acquired pattern quality. The DCF method with subsurface scattering compensation provides better results than the same method without the compensation technique.

calculated standard deviation is roughly $11\times$ greater than the corresponding standard deviation for the DCF method.

4. Discussion

Experimental results show that the presented problem of aligning various materials for laser structuring purposes can be efficiently solved by the presented measurement system. The main difference in comparison with commercially available laser triangulation sensors is the laser beam wavelength. The developed measurement system incorporates a UV laser source characterized by high absorption values in a majority of materials. This is especially critical when measuring translucent and transparent materials, where light in the visible spectrum penetrates through the material surface. In such cases, the measurement result includes a significant bias or the measurement fails completely. Projecting a simple laser dot onto a surface is vulnerable to surface irregularities that affect the reflected signal shape, light intensity distribution, position stability, and other sources of uncertainty as seen in Fig. 1. These effects govern the measurement precision and repeatability. We reduced the measurement dependence on these uncertainty sources by introducing dynamic symmetrical pattern projection. A circle pattern with radius $r = 0.5$ mm is drawn by projecting a laser beam in continuous circular motion with the use of a 2D galvanometric scanning system, as shown in Fig. 3.

A greater measurement area reduces dependence on local surface irregularities, such as scratches or optical discontinuities, whereas dynamic symmetrical pattern projection introduces spatial signal integration. Spatial integration was proven effective for reducing speckle noise and the corresponding measurement uncertainty [3,9], and for producing a Gauss-like light distribution if radial cross sections of the symmetrical pattern are examined. The triangulation angle results in a transformation of the projected circle into an ellipse. In order to obtain a measurement result, a precise centroid position of the acquired ellipse pattern has to be determined. We used the aforementioned geometric pattern properties to introduce a novel centroid detection method; the DCF method. As the name depicts, the method consists of two steps. In the first step, a Gaussian curve is fitted to radial cross sections, which results in robustness to local light intensity variations. In the second step, an ellipse is fitted to points that describe the peaks of Gaussian curves, thus providing the position of the pattern centroid as a result.

Translucent materials present unique measurement problems since the incident light partially penetrates into the surface, causing subsurface scattering. It is assumed that the triangulation angle causes subsurface scattering to be detected as a drop-like shape of the ellipse pattern. The effect of the beam projection angle can be disregarded because

of the telecentric lens we used. A study of radial cross-section profiles reveals that the drop-like effect is defined by a skewed Gaussian-like light intensity distribution. Description of these profiles with an ideal Gaussian curve results in a peak position offset, as shown in Figs. 7 and 8. We introduce a subsurface scattering compensation technique which uses the property of pattern symmetry to reduce measurement dependence on subsurface scattering. The method is based on summations of opposite cross-section profiles with regard to a symmetry line running perpendicular to the viewing axis, which results in a Gaussian-like symmetrical intensity distribution (Fig. 9). The method enables precise centroid position calculation despite nonideal pattern shape and illumination distribution, which is shown in Fig. 4. Furthermore, the method proves robust to various reflection types caused by different surface optical properties (Fig. 10).

Experiments conducted on two different surface types (diffuse and translucent) with varying laser beam intensity confirmed the theoretical background of subsurface scattering compensation. Fig. 11 and Table 2 (Appendix A), which describe measurements of a diffuse material, show that the aforementioned effect does not result in a high measurement bias when using the DCF method without compensation. Nevertheless, the DCF method with included compensation shows lower dependence on laser intensity. Careful consideration of vertical axis boundaries in Fig. 11 reveals that both methods provide excellent measurement performance for diffuse materials, with measurement bias between 1.5 and $-7.0\ \mu\text{m}$, and low, relatively constant standard deviation between ± 0.3 and $\pm 5.3\ \mu\text{m}$. On the other hand, Fig. 12 and Table 3 (Appendix A) show strong dependence on laser intensity when measuring translucent materials with the use of the DCF method without subsurface scattering compensation. The measurement bias, located between -27.6 and $-119.3\ \mu\text{m}$, is governed by varying laser intensity and the corresponding drop-like effect of the acquired pattern. In comparison, the DCF method with subsurface scattering compensation results in superior measurement performance, showing robustness to laser intensity. It can be observed that the measurement bias is described as constant, varying from -17.8 to $-19.4\ \mu\text{m}$. This bias could originate from summation of asymmetric radial cross-section profiles, which are caused by uneven accumulation of light inside the projected pattern (see images in Table 3, Appendix A). Furthermore, negative values indicate that the ellipse centroid was detected inside the material surface. Experiments conducted on different materials, with measurement results presented in Fig. 13 and Table 4 (Appendix A), show that measurement bias is present for all materials. It is dependent on the acquired pattern quality which is governed by material surface optical properties. When the reflected light signal can be described by a thin ellipse with evenly distributed intensity,

Gaussian curves can be fitted with less uncertainty. Both detection methods provide precise measurement results with low bias, ranging from -2.9 to $-13.5\ \mu\text{m}$, and standard deviation, ranging between ± 0.6 and $\pm 1.5\ \mu\text{m}$. Gaussian curves with small standard deviation provide a distinct maximum position, which results in high measurement repeatability. Thick ellipse patterns cause more fitting uncertainty, which results in greater measurement bias, found between -20.9 and $-65.0\ \mu\text{m}$, and higher, less constant standard deviation, ranging from ± 1.6 to $\pm 6.3\ \mu\text{m}$. The conducted experiment clearly shows that measurement precision is close to $z_R/10 \approx 50\ \mu\text{m}$. Furthermore, measurement results for the case of a static laser dot instead of a circle confirm the effect of surface irregularities on measurement precision.

The presented measurement system could be used in measurement applications that demand robustness to material type and partial robustness to surface irregularities. These applications include 3D scanning of various surfaces with a single sensor configuration, material alignment for CNC machining purposes, and various surface inspection procedures. The system is limited to materials that do not react to small doses of UV irradiation. In its current form, it is not suitable for stand-alone commercial use since it utilizes a high-quality UV laser beam and a 2D galvanometric scanning system. The latter has a high price and large dimensions, which are not appropriate for measurements in tight spaces. The main advantage and simultaneously a possible drawback of the presented measurement method is dynamic circle projection. The bigger measurement area could present problems when measuring structures with dimensions smaller than the circle diameter. In such cases, the circle would overlap the structure, causing the circle to deform and introduce additional measurement bias. Furthermore, the acquired pattern shape is dependent on the measured surface tilt. A tilted surface introduces a similar circle transformation as the triangulation angle, with the ellipse orientation corresponding to surface orientation.

5. Conclusion

Robust alignment of a material surface relative to the laser focus position is one of the most important steps in laser structuring applications. It enables the structuring process to be carried out under optimum fabrication conditions, thus resulting in high-quality products. Because contact sensors occlude the laser working area, contactless sensors, where laser triangulation is often used, are utilized for alignment purposes. The PCB manufacturing industry, where a wide spectrum of materials is used at different design stages, presents a problem for commercially available laser triangulation probes since the laser beam is not absorbed equally in different materials. Consequently, a novel contactless displacement







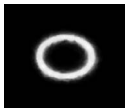
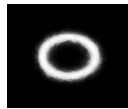
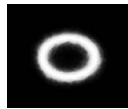

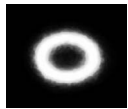

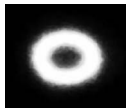

measurement system based on the laser triangulation principle was developed. Measurement of different material types (diffuse, transparent, translucent, and others) is possible by means of an appropriately intensity-regulated high-quality UV wavelength laser beam, primarily used for structuring purposes. Furthermore, a 2D scanning system is utilized for dynamic projection of a symmetrical pattern, which presents a crucial advantage. Dynamic projection results in spatial integration, which is shown to reduce the effect of speckle noise, and the symmetry property results in robustness to local surface irregularities. The centroid of the projected symmetrical pattern is obtained by means of a

novel DCF detection algorithm, which includes subsurface scattering compensation. The latter proves superior when measuring translucent materials where subsurface scattering affects the measurement bias. The presented measurement system performance is dependent on material type. Experimental results have shown that the presented measurement system precision is better than $50\ \mu\text{m}$ for all tested material types, and some materials enable measurement precisions better than $15\ \mu\text{m}$.

The research is partially financed by the European Union/European Social Fund.

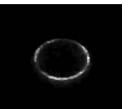

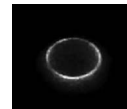
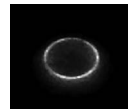
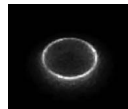


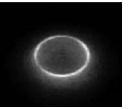
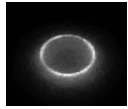
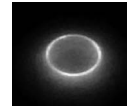
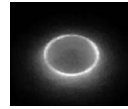
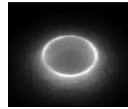

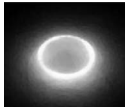
Appendix A

Table 2. Effect of Laser Beam Intensity Variation on Diffuse Material Measurement

Intensity (V)		3.0	2.9	2.8	2.7	2.6	2.5	2.4
No Compensat.	Offset (μm)	-0.0 ± 0.6	-1.3 ± 0.5	-2.4 ± 0.3	-3.0 ± 0.5	-3.6 ± 0.3	-4.8 ± 0.4	-5.6 ± 0.5
Compensation	Offset (μm)	1.5 ± 1.3	0.5 ± 1.0	0.2 ± 1.0	0.6 ± 1.0	-0.5 ± 1.1	-1.6 ± 1.4	0.4 ± 1.3
	Image ^a							
Intensity (V)		2.3	2.2	2.1	2.0	1.9	1.8	1.7
No Compensat.	Offset (μm)	-6.1 ± 0.5	-6.5 ± 0.6	-6.3 ± 0.6	-6.0 ± 0.5	-6.8 ± 0.6	-7.0 ± 0.7	-4.6 ± 1.2
Compensation	Offset (μm)	-1.1 ± 0.9	-1.5 ± 2.7	-4.2 ± 2.6	-2.0 ± 3.3	-5.8 ± 1.9	-1.0 ± 2.7	1.8 ± 5.3
	Image ^a							

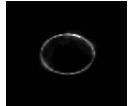
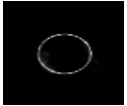

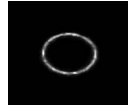
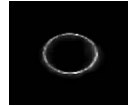
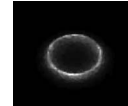
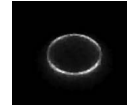
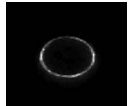
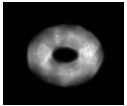
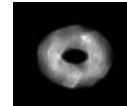
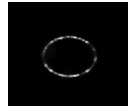
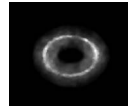
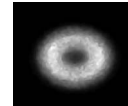
^aBlack and white color shades in the images present low and high light intensities respectively.

Table 3. Effect of Laser Beam Intensity Variation on Translucent Material Measurement

Intensity (V)		2.45	2.4	2.35	2.3	2.25	2.2	2.15
No Compensat.	Offset (μm)	-27.6 ± 1.7	-33.7 ± 3.5	-35.2 ± 3.6	-40.7 ± 5.7	-57.8 ± 3.5	-68.9 ± 5.0	-80.6 ± 7.3
Compensation	Offset (μm)	-19.4 ± 1.4	-19.2 ± 1.5	-19.1 ± 1.4	-19.2 ± 1.2	-19.2 ± 1.2	-18.8 ± 1.1	-18.2 ± 1.2
	Image ^a							
Intensity (V)		2.1	2.05	2.0	1.95	1.9	1.85	1.8
No Compensat.	Offset (μm)	-95.8 ± 5.1	-104.3 ± 3.6	-112.7 ± 1.9	-115.5 ± 2.2	-118.1 ± 2.2	-119.3 ± 2.6	-115.0 ± 4.9
Compensation	Offset (μm)	-17.8 ± 1.0	-18.1 ± 1.2	-18.0 ± 1.0	-18.2 ± 1.0	-18.3 ± 1.1	-19.1 ± 1.0	-18.1 ± 1.3
	Image ^a							

^aBlack and white color shades in the images represent low and high light intensities.

Table 4. Performance of the DCF Method on Different Material Types

Material	Polyimide 50 μm	Polyimide 80 μm	Polyimide 180 μm	White Paper	Cover Layer	FR4 180 μm	FR4 210 μm	
Material type	Transparent	Transparent	Transparent	Diffuse	Transparent	Translucent	Translucent	
Intensity (V)	1.27	1.27	1.17	2.85	1.37	2.45	2.43	
No Compensat.	Offset (μm)	-6.2 ± 0.7	-7.2 ± 1.2	-13.2 ± 0.6	-4.4 ± 0.7	-9.0 ± 0.9	-65.0 ± 2.4	-28.8 ± 1.1
Compensation	Offset (μm)	-3.9 ± 1.0	-7.2 ± 1.5	-13.5 ± 0.8	-3.2 ± 1.1	-2.9 ± 0.9	-28.1 ± 1.7	-20.9 ± 1.6
	Image ^a							
Material	FR4 450 μm	FR4 + Cu New	FR4 + Cu Oxidized	PTFE	Ceramics 350 μm	Ceramics 630 μm		
Material type	Translucent	Specular	Specular	Diffuse	Porous	Porous		
Intensity (V)	2.4	1.48	0.98	1.56	1.96	1.76		
No Compensat.	Offset (μm)	-36.0 ± 1.5	-39.4 ± 1.8	-41.4 ± 2.7	-30.8 ± 0.7	-9.5 ± 1.3	-53.0 ± 1.3	
Compensation	Offset (μm)	-28.9 ± 1.6	-30.0 ± 5.5	-40.7 ± 5.8	-29.6 ± 1.1	-13.9 ± 1.6	-43.5 ± 6.3	
	Image ^a							

^aBlack and white color shades in the images represent low and high light intensities.

References

1. "PCB Prototyping, SMT Stencils, Depaneling, LDS, MID—LPKF Laser & Electronics AG," retrieved August, 2012, <http://www.lpkf.com/>.
2. M.-C. Amann, T. Bosch, M. Lescure, R. Myllylä, and M. Rioux, "Laser ranging: a critical review of usual techniques for distance measurement," *Opt. Eng.* **40**, 10–19 (2001).
3. M. Daneshpanah and K. Harding, "Surface sensitivity reduction in laser triangulation sensors," in *Proceedings of SPIE 8133, Dimensional Optical Metrology and Inspection for Practical Applications* (SPIE, 2011), p. 813300.
4. H. Wang, "Long-range optical triangulation utilising collimated probe beam," *Opt. Lasers Eng.* **23**, 41–52 (1995).
5. J. Liu, L. Tian, and L. Li, "Light power density distribution of image spot of laser triangulation measuring," *Opt. Lasers Eng.* **29**, 457–463 (1998).
6. F. Murakami, "Accuracy assessment of a laser triangulation sensor," in *Advanced Technologies in Instrumentation and Measurement Technology Conference, 1994. IMTC/94. Conference Proceedings. 10th Anniversary* (IEEE, 1994), pp. 802–805.
7. J. C. Dainty, J. W. Goodman, G. Parry, T. S. McKechnie, E. Ennos, and M. Françon, *Laser Speckle and Related Phenomena* (Springer-Verlag, 1984).
8. R. Baribeau and M. Rioux, "Centroid fluctuations of speckled targets," *Appl. Opt.* **30**, 3752–3755 (1991).
9. R. Baribeau and M. Rioux, "Influence of speckle on laser range finders," *Appl. Opt.* **30**, 2873–2878 (1991).
10. R. G. Dorsch, G. Häusler, and J. M. Herrmann, "Laser triangulation: fundamental uncertainty in distance measurement," *Appl. Opt.* **33**, 1306–1314 (1994).
11. B. Muralikrishnan, W. Ren, D. Everett, E. Stanfield, and T. Doiron, "Dimensional metrology of bipolar fuel cell plates using laser spot triangulation probes," *Meas. Sci. Tech.* **22**, 1–12 (2011).
12. B. Muralikrishnan, W. Ren, D. Everett, E. Stanfield, and T. Doiron, "Performance evaluation experiments on a laser spot triangulation probe," *Measurement* **45**, 333–343 (2012).
13. L. Zeng, F. Yuan, D. Song, and R. Zhang, "A two-beam laser triangulation for measuring the position of a moving object," *Opt. Lasers Eng.* **31**, 445–453 (1999).
14. B. Curless and M. Levoy, "Better optical triangulation through spacetime analysis," in *Proceedings of the Fifth International Conference on Computer Vision* (IEEE, 1995), pp. 987–994.
15. G. Manneberg, S. Hertegård, and J. Liljencrantz, "Measurement of human vocal fold vibrations with laser triangulation," *Opt. Eng.* **40**, 2041–2044 (2001).
16. W. W. Zhang and B. H. Zhuang, "Non-contact laser inspection for the inner wall surface of a pipe," *Meas. Sci. Tech.* **9**, 1380–1387 (1998).
17. P. Xu, S. Yao, F. Lu, X. Tang, and W. Zhang, "Mathematical model for light scanning system based on circular laser," *Chin. Opt. Lett.* **3**, 640–643 (2005).
18. P. Schalk, R. Ofner, and P. O'Leary, "Pipe eccentricity measurement using laser triangulation," *Image Vis. Compu.* **25**, 1194–1203 (2007).
19. S.-J. Lee and D.-Y. Chang, "A laser sensor with multiple detectors for free form surface digitization," *Int. J. Adv. Manuf. Technol.* **31**, 474–482 (2006).
20. F.-J. Shiou and M.-X. Liu, "Development of a novel scattered triangulation laser probe with six linear charge-coupled devices (CCDs)," *Opt. Lasers Eng.* **47**, 7–18 (2009).
21. R. Rantson, C. Stolz, D. Fofi, and F. Mériaudeau, "3D reconstruction of transparent objects exploiting surface fluorescence caused by UV irradiation," in *17th IEEE International Conference on Image Processing (ICIP)* (IEEE, 2010), pp. 2965–2968.
22. R. Rantson, C. Stolz, D. Fofi, and F. Meriaudeau, "Optimization of transparent objects digitization from visible fluorescence ultraviolet induced," *Opt. Eng.* **51**, 033601 (2012).
23. K. Žbontar, B. Podobnik, and F. Povše, "Verfahren und Vorrichtung zur berührungslosen Abstandsmessung (Application filed at the German Patent and Trade Mark Office)," 106,613.2 (20 July 2012).
24. C. Donner and H. W. Jensen, "Light diffusion in multi-layered translucent materials," *ACM Trans. Graph.* **24**, 1032–1039 (2005).
25. P. Hanrahan and W. Krueger, "Reflection from layered surfaces due to subsurface scattering," in *Proceedings of the 20th Annual Conference on Computer Graphics and Interactive Techniques* (ACM, 1993), pp. 165–174.
26. H. W. Jensen and J. Buhler, "A rapid hierarchical rendering technique for translucent materials," *ACM Trans. Graph.* **21**, 576–581 (2002).